Atomic layer deposition of TiO2 on porous polysulfone hollow fibers membranes for water treatment

Jeanne Casetta, Danae Gonzalez Ortiz, Céline Pochat-Bohatier, Mikhael Bechelany, Philippe Miele

Atomic layer deposition of TiO_2 on porous polysulfone hollow fibers membranes for water treatment

Jeanne Casetta [1], Danae Gonzalez Ortiz [1], Céline Pochat-Bohatier [1]*, Mikhael Bechelany [1]*, Philippe Miele [1]

[1]Institut Européen des Membranes, IEM, UMR-5635, Univ Montpellier, ENSCM, CNRS, Place Eugene Bataillon, 34095 Montpellier, France

* celine.pochat@umontpellier.fr and mikhael.bechelany@umontpellier.fr

Abstract

Numerous membranes devoted to water treatment are made of Polysulfone (PSF) and can suffer from performance deterioration because of the intrinsic hydrophobicity of this material. Modifying membrane surface allows the engineering of its physicochemical properties and can achieve improved permeability and anti-fouling efficiency by tuning the membrane hydrophilicity or porosity. Atomic layer deposition (ALD) is a unique technology that provides highly conformal and uniform coatings layers such as oxides over surfaces of three-dimensional (3D) parts, porous materials and particles. In this work, titanium dioxide (TiO_2) was deposited on polysulfone hollow fibers (HF) membranes via ALD using $TiCl_4$ and H_2O as precursors. Membranes obtained with increasing number of deposition ALD cycles were tested until the pores were totally blocked. The morphology, structure and mechanical properties of membranes were not altered. The deposition was confirmed by scanning electron microscopy (SEM), Energy-dispersive X-ray spectroscopy (EDX) and X-ray Photoelectron Spectroscopy (XPS) analyses. The deposition of TiO_2 enhanced by 50% the water permeability and by 20% the fouling resistance of the PSF HF membranes until only 20 ALD cycles. This is accompanied by an increase of hydrophilicity and a pores size reduction.

Key words: Membrane, Hollow fibers, Atomic layer deposition, Titanium dioxide, Polysulfone

1. Introduction

During the past few years, fast industrial development and population growth have strongly threatened the ecological environment and human health[1–3]. As surface and underground water have been more and more contaminated, the availability and safety of drinking water became an ongoing global challenge. One of the solutions to counteract this issue is to reuse wastewater. So far, many water purification processes to separate contaminants from water are developed. Indeed, thanks to their many advantages such as high separation efficiency, easy operation, low energy consumption and their environmentally friendly behaviour[4], membranes are among the most advanced ones. Pressure-driven separation processes can be divided in four categories such as microfiltration, ultrafiltration, nano-filtration and reverse osmosis depending on the separation properties like water permeability and selectivity. In recent years, hollow fiber (HF) membranes attracted interest due to their larger specific area, excellent scalability and superior flexibility when compared to flat membranes[5]. Among them, water treatment membranes[6] can be classified, according to their nature, as inorganic membranes when they use ceramics[7,8], zeolites[9,10] or silica materials[11,12]; or as organic membranes based on synthetic polymers such as polyethylene (PE)[13] , polyethersulfone (PES)[14], polyvinylidene fluoride (PVDF)[15], or polysulfone (PSF)[16]. The latter is one of the leading choice for HF membrane fabrication because of its excellent chemical and thermal resistance during membrane washing, and its good mechanical properties suitable for long-term use. However, the main drawback of this polymer is its intrinsic hydrophobicity that affects especially antifouling performances[17]. In order to offset this problematic, modifying membrane surface allows the engineering of its physicochemical properties and can achieve improved permeability and anti-fouling efficiency by tuning the membrane

hydrophilicity, surface charge or porosity[18,19]. Several modification techniques are developed like blending, grafting or mixed-matrix. Govardhan *et al.* prepared PES/Polyetherimide HF membranes by blending method and tested the modules in a laboratory membrane unit for water reclamation. They obtained a pure water permeability at 1 bar twice higher than the initial PES HF membrane reaching also a 99 % Bovine Serum Albumin (BSA) rejection[20]. Cai *et al.* synthesized zwitterionic polymers grafted PES HF membranes for osmotic power generation. They observed that modified membranes exhibited improved fouling resistance to protein and bacterial adhesion without alteration of their morphology. Such systems also achieved higher water flux in pressure retarded osmosis tests compared to initial membrane[20]. Wan *et al.* prepared PVDF HF membranes with UIO-66 metal organic frameworks for arsenate removal in water. They transformed the initial membrane that could not reject arsenate because of the presence of too large pores, into a hydrophilic mixed matrix membrane able to eliminate arsenate by sorption on UIO-66[21]. Another possibility for surface modification is the use of coating method, which consist in depositing a thin layer of material on the membranes' surface. Different techniques[22] can be used, such as sol-gel, physical vapor deposition (PVD), chemical vapor deposition (CVD) or atomic layer deposition (ALD). Dong *et al*. synthesized PVDF/Al_2O_3 hybrid membrane *via* sol–gel process. They obtained a pure water flux increased by 83.4 % between the initial and modified membranes while the BSA rejection was improved from 88.3 to 96.6 %[23]. Kowalik-Klimczak *et al.* modified polyamide membranes with copper oxide using PVD techniques. They achieved a stable coating during filtration of demineralized water and the modified membranes showed a strongest bactericidal activity, which allowed eliminating 99% of microorganisms[24]. Nomura developed silica membranes by CVD method on a porous ceramic substrate with controlled pore sizes and hydrothermally stable for the steam reforming reaction to extract H_2[25]. All of these methods are interesting and provide promising results but ALD stands out from the crowd thanks to its very high surface conformality. Where PVD concerns only the surface , sol-gel blocks the pores and CVD will not provide a uniform layer all along, the surface-controlled film growth of ALD allows the obtaining of highly uniform coatings over surfaces of three-dimensional (3D) parts, deep trenches, porous materials and particles[26]. ALD is in fact one of the most recent techniques, a unique technology developed over the last four decades[27], which allows the deposition of inorganic coating layers such as oxides; for example iron oxide FeO[28], aluminium oxide Al_2O_3[29], lanthanum oxide La_2O_3[30], silica SiO_2[31] or tin oxide SnO[32]; with high uniformity and precise sub-nanometer thickness control.

As an environmental-friendly, low-cost and highly hydrophilic oxide, titanium dioxide TiO_2 can be advantageously used for modifying membrane surface properties[33]. Hamid *et al*. incorporated TiO_2 nanoparticles into PSF HF membranes and observed a diminution of water contact angle (WCA) from 75° for raw membranes to 45° for TiO_2 modified membrane. They also proved great antifouling properties against humic acid with a twice higher flux and a better flux recovery from 90 % to 95 %[34]. Nechifor *et al*. produced polysulfone-silica microfiber grafted with TiO_2 nanoparticles composite membranes. They obtained a 94% retention of BSA and a water permeability increase of 45%, as long as a great anti-bacterial action for PSF/SiO_2 + TiO_2 composite membranes[35].

Recent studies have shown that ALD is applicable to flexible and temperature-sensitive polymeric membranes[36,37], the deposition of an oxide thin layer could increase the membrane hydrophilicity, modify its pore size and reduce the membrane fouling despite sacrificing the water permeability. Actually, some reviews are focused on the sensitization of nominally unreactive membrane materials for subsequent ALD and the use of ALD oxides as a hydrophilization coating on membranes. Yang *et al.* reviewed ALD/ sequential infiltration synthesis (SIS) engineering strategies with realization of efficient water treatment. They laid out a pathway to establish an ALD/SIS-based universal functionalization platform for water treatment, including sensitization strategies.[38] Wu *et al.* summarized the most recent advances in molecular engineering to tailor the properties of interfaces in composite membranes. They explained how the performances of membranes can be enhanced by the way of several surface modification techniques.[39] Yang *et al.* discussed the application of ALD and related techniques in the design of novel membrane interfaces and explained how ALD can be used for instance to modify the surface chemistry and interfacial properties of membranes and tailor the pore sizes.[40] Feng *et al.* proceeded ALD of ZnO on carbon nanotubes. For 40 cycles they observed the highest

permeability value at 430 $L.m^{-2}h^{-1}bar^{-1}$, a WCA reduced by a third and a six time higher BSA rejection. However, for more than 40 cycles the permeability decreased and the WCA did not change[41]. Wang *et al.* deposited polyimide on the surface of nanoporous anodized alumina by ALD. They showed that 50 cycles lead to the remarkable upgrade of retention from nearly none for the neat alumina substrate to 82 % while the water permeability almost three time lower was still maintained as high as 800 L/hm^2bar[42]. The interest in using ALD technique on polymers is growing for different type of applications such as in barrier materials, protective coatings and gas and liquid filters. The mechanisms and reactions occurring during ALD process on some polymers had been studied by Parsons *et al*. They focused particularly on the common Al_2O_3 reaction sequence using trimethyl aluminum (TMA) and water on different kind of polymers such as polypropylene (PP), polyamide or polyester. They explained that reaction during TMA/H_2O deposition on polymer materials depends strongly on the starting polymer, the precursor as well as the detailed process conditions. With inert polymer like PP, the TMA diffuses into the near surface region of the polymer and will then react with water during the second half-cycle step to form nuclei beneath or at the polymer surface. On polymers where there is a large density of reactive groups, the ALD reaction can be limited to the top surface of the polymer. Carbonyl site is the most Lewis basic functionality in some polymers, so it is expected to coordinate with the TMA Lewis acid to form an aluminum-oxygen-alkyl unit and to disrupt the hydrogen bonding between neighboring chains, which could act to "open up" the polymer chain network, promoting further TMA diffusion into the subsurface region. Like TMA, $TiCl_4$ is also a strong Lewis acid, so it may diffuse into the polymer and react with it through similar Lewis acid/base adducts[43]. To the best of our knowledge, there are several articles that focused on the insertion of TiO_2 onto PSF membranes[34,44–47] or on the deposition of oxides on polymeric membranes[48,49] but there is no study focusing on TiO_2 ALD on PSF HF membranes.

This study focus on the surface modification of PSF HF membranes by TiO_2 using ALD technique and its influence on the fiber properties compared to raw PSF HF membranes. The effect of ALD treatment on the membrane morphology was investigated by scanning electron microscopy (MEB) and in terms of hydrophilicity and pores size. The performances of the HF membranes for water purification application were characterized: water permeability, antifouling using Bovine Serum Albumin (BSA) protein and mechanical properties. The modification of polymeric membranes by ALD requires a preliminary step of conditioning to enable them to withstand vacuum under heat treatment. To the best of our knowledge, there has not yet reported studies in the literature clarifying the conditioning of polymeric membranes for TiO_2 deposition by ALD on PSF HF membranes. So in a first step, we will present the glycerin conditioning of the membrane and then the effect of deposition of 10, 20, 50 and 100 cycles TiO_2 on the membrane structure and properties.

2. Materials and methods

2.1. Materials

PSF HF membranes supplied by Polymem were used as substrates for TiO_2 ALD. The membranes were received after chlorine washing and glycerin conditioning steps. Titanium (IV) chloride ($TiCl_4$, 99.9%, CAS: 7550-45-0) and deionized water were served as metallic and oxygen source for the ALD process, respectively. Argon gas was bought from Linde and used as received. Phosphate buffered saline (PBS) (Roth) and bovine serum albumin (BSA) (Mw=67 kDa, ≥96%, Sigma-Aldrich) solution were employed to assess the fouling resistance of both raw and modified PSF HF membranes. Dextran (M_w from 6 to 2,000 kDa, Sigma-Aldrich) were used for membrane pore size characterization. Deionized water (Millipore Milli-Q) was used in all aqueous solutions.

2.2. TiO_2 ALD on PSF HF membranes

The commercial PSF membranes were received conditioned in a water/glycerin mixture. This processing is usually applied in industry to preserve the porous structure along storage. The glycerin must then be removed when the membranes are in use. Membranes called P, P-0 and P-10 have been washed in successive water baths to remove glycerin before experiments. Membranes called P-g-0, P-g-10, P-g-20, P-g-50 and P-g-100 undergone ALD process as received. After deposition, they were washed in successive water baths to remove glycerin to determine their functional properties. The commercial PSF membranes were introduced for a 15 min acclimation in the home-built ALD reactor under vacuum (~10^{-2} mbar) and preheated at 100°C. The deposition process was achieved using $TiCl_4$ and H_2O as precursors contained in stainless steel cylinders which lines were heated at 80°C to avoid condensation. One ALD cycle consisted of 50 ms pulse of $TiCl_4$, followed by 10 s exposure and 60 s purge with Ar gas, then H_2O valve was opened for 2 s, followed by an exposure of 10 s and purge for 60 s. Several cycles were applied 10, 20, 50 and 100 that correspond respectively to 1, 2, 5 and 10 nm thick deposit according to a previous study conducted in this ALD chamber and using these operating conditions[50].

Table 1 presents the nomenclature of the PSF HF membranes that have undergone the different tests of this study.

Table 1: Membranes nomenclature (All membranes, except from P and P-g, were introduced in ALD chamber for a 15 min vacuum acclimation at 100°C)

Fiber's name	**Description**
P	PSF industrial fiber reference washed to remove glycerin
P-0	PSF industrial fiber washed and placed in the ALD chamber under vacuum and at 100°C during 25 min without deposition
P-g	PSF industrial fiber reference conditioned with a water/glycerin mixture
P-g-0	PSF industrial fiber conditioned with glycerin placed in the ALD chamber under vacuum and at 100 °C during 25 min without deposition
P-10	PSF industrial fiber placed in the ALD chamber under vacuum and at 100 °C during 25 min for TiO_2 deposition (10 cycles corresponding to 1 nm thickness)
P-g-10	PSF industrial fiber conditioned with glycerin placed in the ALD chamber under vacuum and at 100 °C during 25 min for TiO_2 deposition (10 cycles corresponding to 1 nm thickness)
P-g-20	PSF industrial fiber conditioned with glycerin placed in the ALD chamber under vacuum and at 100 °C during 1 h for TiO_2 deposition (20 cycles corresponding to 2 nm thickness)

P-g-50	PSF industrial fiber conditioned with glycerin placed in the ALD chamber under vacuum and at 100 °C during 3 h for TiO_2 deposition (50 cycles corresponding to 5 nm thickness)
P-g-100	PSF industrial fiber conditioned with glycerin placed in the ALD chamber under vacuum and at 100 °C during 8 h for TiO_2 deposition (100 cycles corresponding to 10 nm thickness)

166

167 **2.3. Characterizations**

168 The morphology of the membrane, both cross-section and surface, was observed using a Hitachi S4800
169 scanning electron microscopy system (SEM) after previous nitrogen cold-cutting. Energy-dispersive X-
170 ray spectroscopy analysis (EDX) was performed with a Zeiss EVO HD15 microscope coupled with an
171 Oxford X-MaxN EDX detector. To investigate the changes in chemical structure and to confirm the
172 successful deposition of TiO_2 between the raw and the modified PSF HF membranes, Fourier Transform
173 Infrared (FTIR) spectra were acquired using FTIR spectrometer NEXUS instrument equipped with an
174 attenuated total reflection (ATR) accessory in the frequency range of 600–4000 cm^{-1}. The ATR-FTIR
175 spectra were recorded with a resolution of 4 cm^{-1}, and the signals were averaged from 64 scans. The
176 mechanical properties of the raw and modified PSF HF membranes were characterized using a dynamic
177 mechanical analysis device (Z005, 5 kN Proline, Zwick Roell). A 10N sensor and a tensile testing speed
178 of 0.4 $mm \cdot min^{-1}$ were applied. The Young's modulus of the membranes was calculated directly from
179 the device. Water contact angles (WCA) were measured using a tensiometer/goniometer ILMS GBX,
180 equipped with an optic telecentric F55 double focal monochrome and a GBX software. For each
181 sample, about 0.5 µL of ultrapure water was deposited on the membranes using a needle.
182 Furthermore, X-ray Photoelectron Spectroscopy (XPS) was carried out with a Kratos AXIS NOVA
183 spectrometer (Kratos Analytical Ltd., Manchester, UK) using a monochromatized Al Kα X-ray source
184 (1486.6 eV) operating at a power of 150 W (10 mA, 15 kV). Survey and high-resolution spectra were
185 acquired at 160 and 20 eV pass energies, respectively. Mean pore diameter of raw HF membrane had
186 been kindly determined by Porometer using the liquid-liquid porometry on a POROLIQ 1000ML.

187

188 **2.4. Filtration experiments**

189 A U-tube shaped hollow fiber bundle which consisted of 10 wet fibers measuring each 40 cm long
190 (equivalent to 90 ± 5 cm^2 effective membrane area) was prepared using a homemade polyvinyl chloride
191 (PVC) housing module. Epoxy resin was used to seal the module. The pure water flux (J_w) was measured
192 for each membrane by circulating pure water through the membrane system using an applied pressure
193 range of 0.5–1.5 bar. Each point was obtained measuring the flow passing through the membrane
194 during 60 s. The pure water flux, J_w ($L.h^{-1}m^{-2}$), was calculated using the following formula:

195 $$Jw = \frac{Q}{A}\ (L \cdot h^{-1} \cdot m^{-2}) \qquad (1)$$

196 where Q ($L \cdot h^{-1}$) is the amount of water that passed through the membrane and A (m^2) is the membrane
197 area. The permeability was determined from the slope of the linear variation of J_W versus the applied
198 pressure.

Rejection experiments were conducted to estimate the pore size and their reduction after ALD using 1 g/L aqueous solutions of Dextran solutes with M_w going from 6 to 2,000 kDa. A U-tube shaped hollow fiber bundle was prepared like described above. Dextran contents in the feed (C_f) and in the permeate (C_p) solutions were determined by flow injection analysis using refractometer 2414 (Waters Corporation). The solute rejection (R) was calculated using the following formula:

$$R = 1 - \frac{C_p}{C_f} \times 100\ (\%) \tag{2}$$

The membrane was first conditioned by applying a pressure of 1.5 bar with distilled water for 30 minutes. External-internal solute filtration of the membrane was then carried out for 20 min at 0.5 bar. The hydrodynamic radius values, r_p in Å, of the various Dextran molecules used in these experiments were estimated from the following equation[51]:

$$r_p = 0.488\, Mw^{0.437} \tag{3}$$

where M_W is the molecular weight of the Dextran.

Static protein adsorption was performed to estimate the anti-fouling properties of the TiO_2-deposited PSF HF membranes and the raw PSF HF membrane was used as reference. An I-shaped hollow fiber bundle, consisting of 10 wet fibers measuring each 27 cm long (equivalent to an effective membrane area of 63.28 cm^2), was prepared using a polyvinyl chloride (PVC) module and an epoxy resin as sealing agent. The protein solution was prepared by dissolving 2 g of BSA in 2 L of PBS solution at pH 7.4. The membrane was first conditioned by applying a pressure of 1.5 bar with distilled water for 30 minutes. Initial external-internal water filtration of the membrane is then carried out for 20 min at 0.5 bar and the steady pure water flux was recorded (Jw_0) using a balance and data acquisition software. The tank was then filled with the BSA solution and filtration was carried out at 0.5 bar for 2 hours and foulant flux was recorded (Jw_f). The BSA was removed by mechanical agitation and then backwashing with water applying a pressure of 1.5 bar internally-externally for 5 min. Finally, a last external-internal filtration cycle with water for 20 min at 0.5 bar was performed and the steady flux was recorded (Jw_1). The total fouling ratio (R_t), flux recovery ratio (FRR), the reversible fouling ratio (R_r) and the irreversible fouling ratio (R_{ir}) were estimated using equations (2)–(5), respectively[52]:

$$R_t = \frac{J_{w_0} - J_{w_f}}{J_{w_0}} x100\ (\%) \tag{4}$$

$$FRR = \frac{J_{w_1}}{J_{w_0}} x100\ (\%) \tag{5}$$

$$R_r = \frac{J_{w_1} - J_{w_f}}{J_{w_0}} x100\ (\%) \tag{6}$$

$$R_{ir} = \frac{J_{w_0} - J_{w_1}}{J_{w_0}} x100\ (\%) \tag{7}$$

The feed BSA solution, BSA retentate and permeate concentrations are calculated from Beer Lambert's Law using the constant k = 0.6439 L/g and an ultraviolet (UV) spectrometer on the absorbance at 280 nm (Uviline Connect Series 940). The rejection of protein was obtained from equation (2) where C_p and C_f are the protein concentrations of BSA in permeate and feed.

3. Results and discussion

3.1. Glycerin conditioning

The successful deposition of TiO_2 by ALD on HF membranes is challenging because of the temperature and pressure sensitivity of the polymers. A first study was carried out to observe the influence of glycerin conditioning on the morphology and water permeability of membranes after the deposition of TiO_2. It is necessary to know whether the glycerin brings a protective effect to the polymeric membranes that underwent ALD process. The internal and external diameters of the membranes as well as their lengths were measured before and after ALD treatment. It can be seen that the diameters and lengths are not affected by vacuum (~10^{-2} mbar), temperature (100°C) and TiO_2 deposition as the values before and after are nearly identical. SEM images of the PSF HF membranes cross sections are presented in Fig. 1. All fibers present a sponge-like asymmetric structure characteristic of HF membranes.

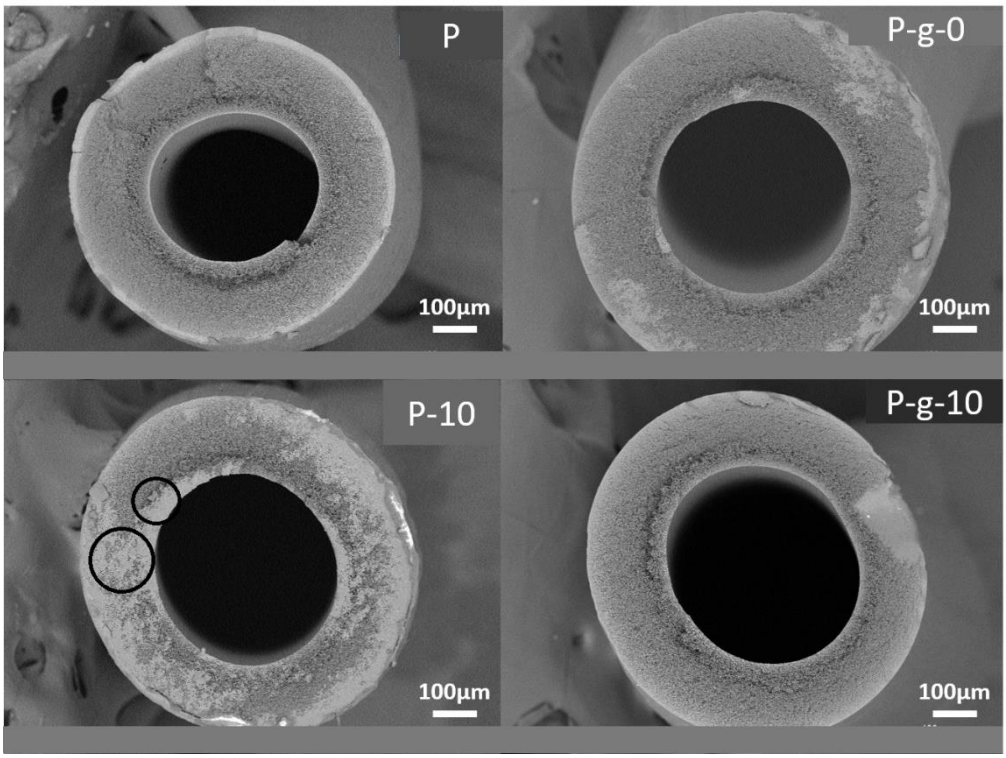

Figure 1. SEM pictures of raw PSf HF (P), PSf HF with 10 ALD cycles (P-10) and PSf HF conditioned with glycerin and with 10 ALD cycles (P-g-10)

In the case of P-10 (without glycerin), SEM images show that most of the pores have collapsed during the deposition, which some are pointed out by the circles, whereas for P-g-10 (sample with glycerin) it is not possible to distinguish any significant change comparing to the raw PSF HF membrane. We assume that glycerin originating from conditioning and settled in the pores of the fiber allows protecting the structure during the preheating (100 °C) and under vacuum acclimation (~10^{-2} mbar). Without glycerin, the HF structure is damaged by temperature and vacuum. No other difference was noticeable between raw and TiO_2 deposited membranes on SEM images. The mean pore diameter of the raw PSF HF membrane was determined by liquid-liquid porometry to be 25 nm. It was believed that ALD deposition may reduce the pore size[48] which was not possible to quantify *via* this technique

as they are too small. Pore size reduction will be evaluated in the last part of this paper using dextran rejection.

The necessity of glycerin conditioning was also evidenced by the results of permeability measurements presented in Table 2. On one hand, membranes without glycerin conditioning P-0 and P-10 display a very low permeability (5±1 and 4±1 $L/h^{-1}m^{-2}bar^{-1}$ respectively) after ALD process. In accordance with SEM images, the deposition damaged the structure of the membrane leading to the collapse of the pores and thus the diminution of water permeability. On the other hand, the glycerin allowed P-g-10 to show a 26 % higher permeability around 170 L/hm^2bar against 135 L/hm^2bar for raw membrane P. The 27 L/hm^2bar permeability of P-g-0 pointed out that glycerin is no longer able to prevent the pore collapsing during the whole vacuum time residence. In fact, as presented in Table 2, P-0 and P-g-0 membranes spent the most time in the ALD chamber under vacuum: 40 min against 15 min for P-10 and P-g-10. So during the fifteen first minutes, the glycerin managed to counteract the pore reduction under vacuum at 100°C, then it is fully evaporated and the membrane structure is altered for the twenty-five other minutes. This explains the drop in permeability for P-g-0. For P-g-10, after the 15 min vacuum acclimation at 100°C, the deposition started and vacuum was stopped.

Table 1 : Water permeability values of P, P-0, P-g-0, P-10 and P-g-10 membranes (the error referred to standard deviation of 3 samples)

Fiber's name	Residence time under vacuum (min)	Residence time with TiO_2 deposit (min)	Permeability ($L/h^{-1}m^{-2}bar^{-1}$)
P	0	0	135 ± 14
P-0	40	0	5 ± 1
P-g-0	40	0	27 ± 4
P-10	15	25	4 ± 1
P-g-10	15	25	170 ± 17

According to SEM pictures and water permeability measurements, the efficiency of glycerin conditioning has been clearly proved. Moreover, the acclimation period before ALD cycles process was a key parameter to allow a good TiO_2 deposition. Several tests have been performed and it was observed that, even for HF with glycerin, an acclimation time superior to 15 minutes deteriorate the HF membrane. After more than 15 minutes in the ALD chamber under vacuum at 100°C, the HF was totally dried and the result is a water permeability close to zero. This proved that glycerin conditioning is efficient only coupled with an acclimation no longer than 15 minutes. Indeed, the boiling temperature of glycerin was reduced from 290°C at atmospheric pressure to 96°C at the pressure applied during deposition (10^{-2} mbar)[53]. We can propose that all the glycerin available on the HF surface is evaporated and only a few amount bounded onto the pores maintain the internal morphology at the end of acclimation at 100°C. The evaporation of glycerin was proved in Fig. 2 (a) with FTIR analysis. Indeed, pure glycerin showed two signals between 2800 and 3000 cm^{-1} corresponding to C-H stretching and one broad and intense band around 3300 cm^{-1} corresponding to O-H stretching. Three fibers were analyzed, the PSF industrial fiber reference conditioned with glycerin P-g, the PSF industrial fiber conditioned with glycerin placed in the ALD chamber under vacuum and at 100°C during 10 cycles for TiO_2 deposition P-g-10 and the PSF industrial fiber reference washed after conditioning. The band

around 3300 cm^{-1} also corresponds to water but the three fibers have been placed in a 60°C oven overnight before analysis, which lead to water evaporation as shown by the P spectrum (washed membrane containing no glycerin). The absorption band at 3300 cm^{-1} is not visible anymore. P-g spectrum presents the same O-H pic than glycerin but less intense whereas P-g-10 did not show any pic in this area. Therefore, it can be concluded that 15 min acclimation in the ALD chamber at 100°C under vacuum eliminate all the glycerin by evaporation as the IR characteristic signals of glycerin have disappeared of the sample after deposition. When the TiO_2 deposition started, $TiCl_4$ reacted directly with PSf support.

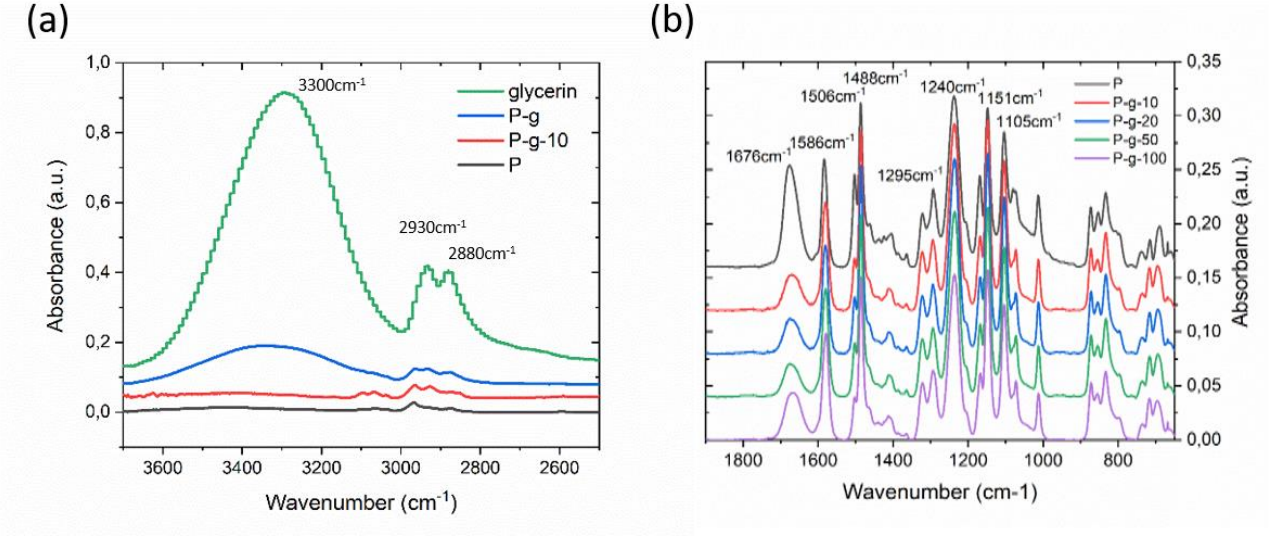

Figure 2. (a) Comparison of ATR-FTIR spectrum of glycerin with those of PSF membrane with glycerin (P-g), washed PSF membrane (P) and PSF membrane with glycerin after 10 ALD cycles and (b) Raw and ALD modified PSF membranes ATR-FTIR spectra

Based on these observations, glycerin conditioning and 15 min acclimation were applied for all the following ALD tests.

3.2 Influence of ALD cycles on membrane properties

3.2.1 Structural and physico-chemical characterizations

The formation of TiO_2 layers on the PSF HF membranes was investigated by ATR-FTIR spectroscopy. In Fig. 2 (b), the characteristic IR peaks of PSF are visible in raw and modified membranes. Signals observed at 1105, 1488, 1506 and 1586 cm^{-1} correspond to the vibrations of PSF aromatic ring (C=C stretching). Bands at 1151 cm^{-1} and 1240 cm^{-1} were attributed to the –O–S–O– symmetric and aromatic ether bond (–C–O–C–), respectively. The peak at 1295 cm^{-1} was related to SO_2 group stretching vibration[54]. Additionally, absorbance peak at 1676 cm^{-1} could be attributed either to the C=O stretching vibration of NMP or PVP that might remain on the membrane surface. Any new peaks could be observed for the ALD modified membranes in the investigated frequency range. Thus we can assume that the amount of TiO_2 is too low to be detected *via* this technique, as a consequence of a low number of ALD cycles. Actually, Jia *et al.* studied the deposition of Al_2O_3 on porous polypropylene HF by ALD technique, and they only noticed a new absorption peak after more than 100 deposition cycles[49].

Moreover, Wang *et al.* studied the deposition of TiO_2 by ALD on PVDF membranes and they suggested that the pic intensity was similar under 100 deposition cycles and began to drop after, as the number of ALD cycles increased. The TiO_2 coating layer may reduce the depth that the light beam can reach in the material, thus the detected IR signal of the PVDF membrane is weaker.[48] The same trend is observed for our samples, the intensity of the peaks decreases when increasing the number of ALD cycles. Any evidence of the deposition of TiO_2 on the PSF HF membranes using ALD technique was found by ATR-FTIR spectroscopy technique. In addition, Waldman *et al.* focused on the SIS of Al_2O_3 in PES membranes and were able to understand the molecular interactions during ALD process through FTIR experiments. They explored in situ FTIR of TMA in-diffusion and out-diffusion to elucidate the nature and kinetics of an attractive interaction between the TMA and the PES moieties. All their FTIR measurements allowed them to confirm that TMA associates with the sulfonyl and aryl ether groups of the PES polymer in a qualitatively similar way to the association with the carbonyl and ester groups of PMMA.[55] This study could help us understanding the molecular interactions that took place in our ALD process supposing that TiO_2 may react with sulfonyl and ether groups of the PSF membrane.

SEM analyses performed on the top surface of raw PSF HF membrane P, and modified PSF HF membranes are presented in Fig. 3. They showed that for raw PSF HF membrane P and the membrane that undergone 10 cycles ALD no change was observed on the surface, which supposed a thin and uniform coating. However, for the PSF HF membrane with 50 ALD cycles, P-g-50, a geometric and regular structure on surface was observed most likely corresponding to the TiO_2 thicker layer that may have cracked. Similar micrographs were obtained for P-g-100.

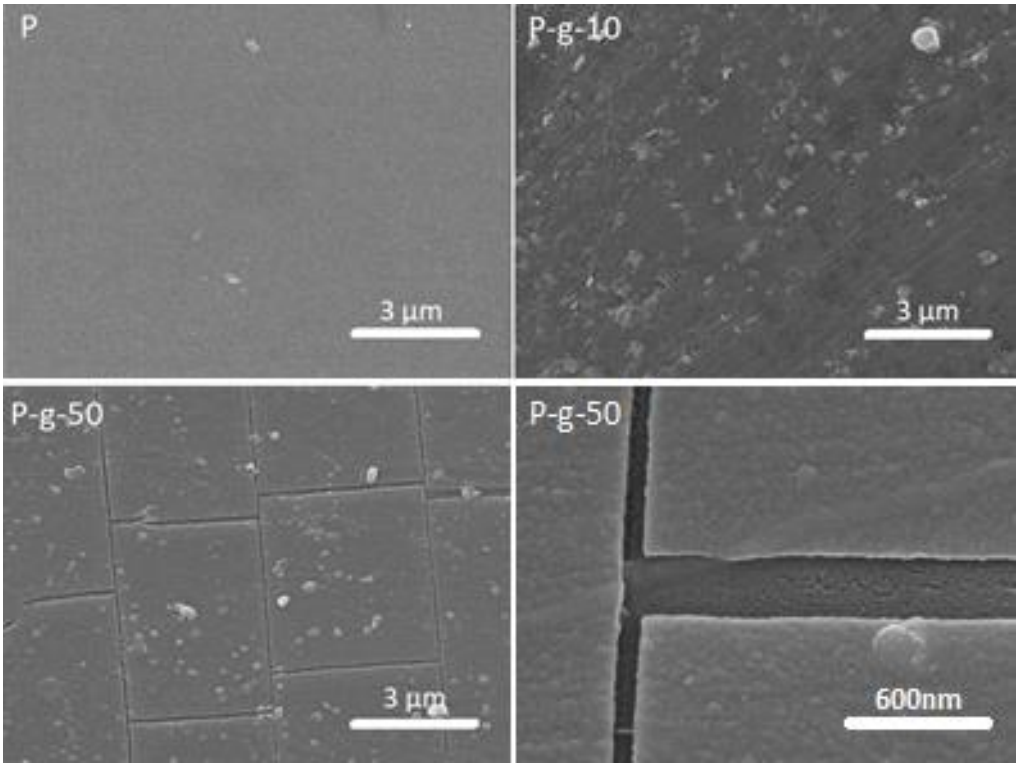

Figure 3. SEM Images of raw (P) and ALD modified membranes surface (10 and 50 cycles)

In order to quantify the amount of TiO_2 deposited on membranes, EDX of all raw and ALD modified PSF HF membranes was performed. The measured atomic percentages of C, O and Ti are presented in Table 3. The detected atomic percentages of Ti were very low for P-g-10 and P-g-20 samples (≤ 0.1) due to small layer thicknesses of TiO_2 (1 and 2 nm respectively), but the Ti atomic percentage increases for P-g-50 and P-g-100 following the increasing number of ALD cycles. These results are in good agreement with SEM observations which allow the observation of the deposit starting from 50 ALD cycles. Moreover, we can add from EDX cross-sectioned mapping in Fig. S1 and Fig. S2 that TiO_2 was uniformly deposited onto the membrane network.

Table 2. EDX data showing the composition of the raw and ALD modified membranes (the error was calculated based on a 10% EDX measurement uncertainty)

Atomic percentages (%)			
Samples	C	O	Ti
P	86.8 ± 8.6	9.9 ± 0.9	0
P-g-10	86.3 ± 8.6	11.3 ± 1.1	≤ 0.1
P-g-20	87.2 ± 8.7	9.9 ± 0.9	≤ 0.1
P-g-50	76.8 ± 7.7	20.5 ± 2.1	0.8 ± 0.1
P-g-100	74.7 ± 7.5	22.2 ± 2.2	1.2 ± 0.1

To go further, XPS analyses were performed on raw and modified membranes. No difference was observed between raw and P-g-10 and P-g-20. We assumed that, according to the other analyses methods, for 10 and 20 ALD cycles the amount of TiO_2 was too low and under the detection limit. P-g-50 and P-g-100 presented the same spectra. The survey of C 1s, O 1s and Ti 2p deconvoluted spectra of P and P-g-50 are presented in Fig. 4. The XPS survey spectra of both membranes (Fig. 4a) consist of two peaks at the binding energies of 284.85 and 532.05 eV assigned to C and O atoms respectively with an additional peak around 458.36 eV for P-g-50 assigned to Ti atom. The C signal in the high-resolution spectra of the raw membrane P could be deconvoluted into three peaks (Fig. 4b): Carbon atoms attached to hydrogen/carbon, sulfone and ether groups exhibit C 1s core-level binding energies of 284.80, 286.20 and 287.90 eV respectively. The C 1s spectra of P-g-50 (Fig. 4d) was similar which supports that the PSf matrix was not damaged during deposition. However, the deconvoluted spectra of O 1 s included two peaks for P (Fig. 4c) at 532.70 and 531.75 eV corresponding to O-C and O=S bonds respectively while a third peak appeared for P-g-50 (Fig. 4e) at 529.86 eV corresponding to the O-Ti bond. This confirmed that TiO_2 was well deposited and reacted with the oxygen atoms of the PSf matrix. For P-g-50, in the deconvoluted Ti 2p spectra (Fig. 4f), two peaks are positioned at 458.36 and 464.16 eV, corresponding to Ti $2p_{3/2}$ and Ti $2p_{1/2}$ states indicating that Ti is 4+ valence.

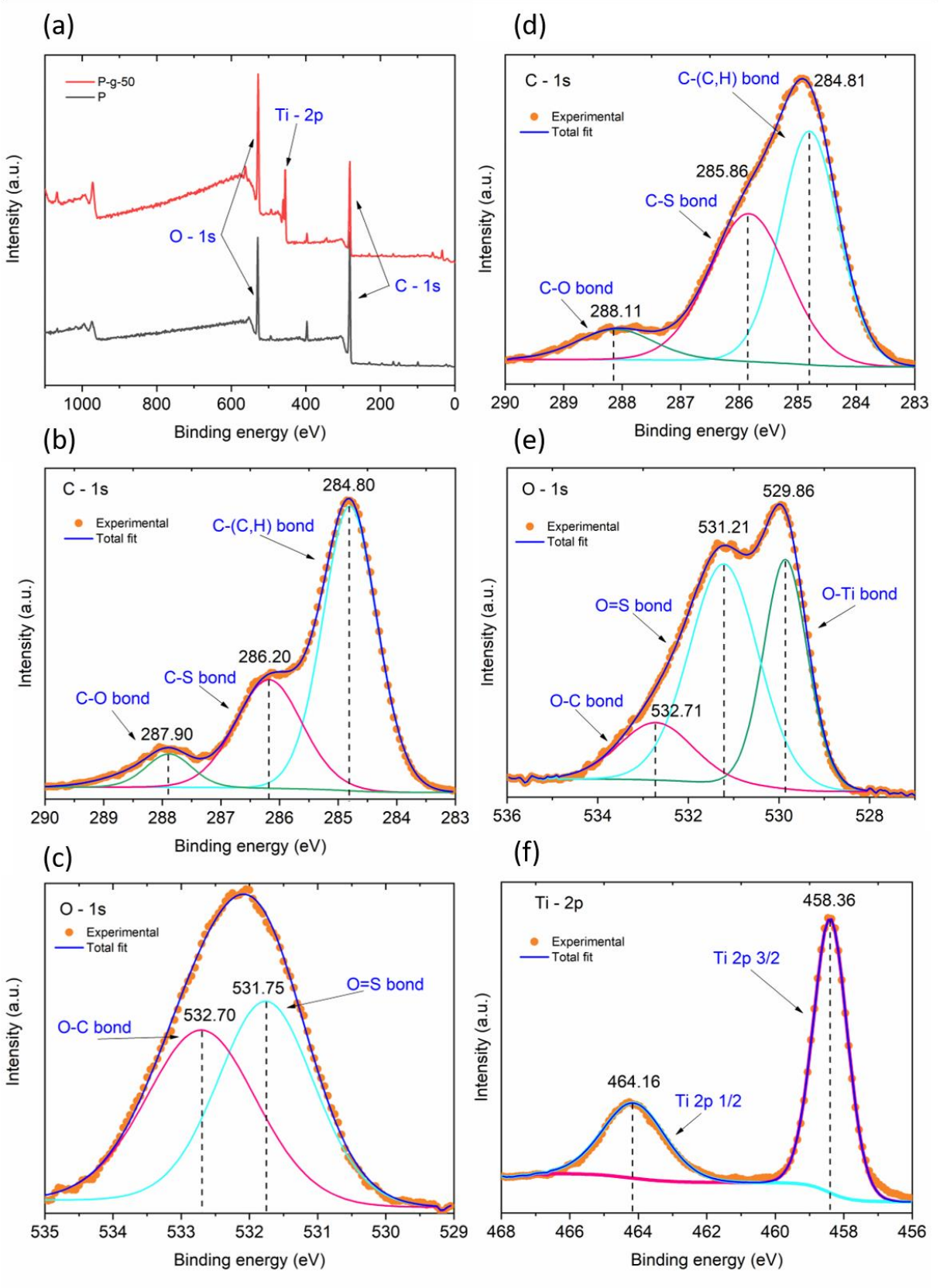

Figure 4: Survey XPS spectra (a) and deconvoluted XPS spectra of P C 1s (b) and O 1s (c) and P-g-50 C 1s (d), O 1s (e) and Ti 2p (f)

3.2.2 Membrane performances

Mechanical tests were performed on raw and modified membranes. Young modulus and the strength at break values are presented in Table 5. The results showed that ALD-modified membranes displayed a higher Young modulus around 147 MPa in average compared to raw membrane (132 MPa), which corresponds to a lower resistance to stress deformation. Any correlation between the increasing number of ALD cycles and the increase Young modulus has been noticed. Because the ALD modified membranes were more rigid, the strength applied to break them was lower than for raw PSF HF membrane decreasing from 2.10 ± 0.02 to in average 1.76 N. However, TiO_2 could act as crosslinker between the polymer chains, improving consequently the rigidity of the network and therefore, the mechanical strength[56]. This observation is in accordance with Diez-Pascual *et al*., who studied the effect of TiO_2 nanoparticles insertion on the performance of polyphenylsulfone. They observed a gradually increasing Young's modulus upon raising nanoparticle loading, by up to 62 % at the highest concentration tested. They attributed this improvement to the effect of the rigid TiO_2 with the interactions (H-bonding) it established with the membrane matrix. This results in a decrease in polymer chain motion and in promoting the adhesion between the two phases[57]. In Table 4 are also presented the permeability values which matched with the SEM observation. In fact, a thin and uniform TiO_2 layer on the membrane surface for P-g-10 and P-g-20 allowed a 26 to 50 % higher permeability value compared to raw membrane P. However, starting from 50 cycles when the coating was thicker a drastic drop in permeability is observed. From these results, 50 and 100 cycles could be discriminated, supposing that the layer is too thick to allow great performance. For the rest of the study, P-g-100 was forsaken and P-g-50 was still studied to compare with P-g-10 and P-g-20.

Table 4. Tensile properties of raw and ALD modified HF membranes (the error referred to standard deviation of 3 samples)

	Young Modulus (MPa)	Strength at break (N)	Permeability (L/hm^2bar)
P	132 ± 5	2.10 ± 0.02	135 ± 14
P-g-10	153 ± 9	1.72 ± 0.11	170 ± 17
P-g-20	143 ± 6	1.84 ± 0.05	200 ± 20
P-g-50	144 ± 4	1.76 ± 0.06	15 ± 2
P-g-100	150 ± 6	1.71 ± 0.08	< 1

SEM did not permit to measure the pore size reduction reported in other works[48]. To complete, different sizes of dextran were filtered through raw and ALD modified PSF HF membranes (P-g-10 and P-g-20). The evolution of the rejection rate versus molecular weight of dextran molecules is presented in Fig. 5 (a). The correspondence between the molecular weight and the pore diameter of dextran molecules was calculated based on Equation (3) and is presented in Table 5. All dextran molecules were able to pass through the raw PSF HF membrane pores from a rejection rate near zero for the smallest molecule to 80% rejection for the biggest at 55.3 nm. It can be observed that even if the mean pore size of raw PSF HF membrane was measured at 25 nm, there is a large distribution that allows molecules up to 55.3 nm going through the membrane. On the other side, P-g-10 presented already 20% rejection rate for smallest dextran at 4.7 nm, 50% for 10 nm sized molecules and reached 90% for 30.2 nm dextran. P-g-20 follows the same trend. Other works from the literature gathered in Table 6 confirmed a noticeable reduction of pore size and pore size distribution after ALD process. Dextran

rejection rates support SEM observations to evidence the deposition of TiO_2 on all the PSF HF membrane surface and subsurface.

Table 5. Correspondence between molecular weight and hydrodynamic radius values of dextran molecules

M_w (Da)	6.10^3	4.10^4	10^5	2.10^5	5.10^5	2.10^6
r_p (nm)	4.7	10	14.9	20.2	30.2	55.3

It is well known that surface hydrophilicity affects the membranes antifouling properties. Membranes' WCA were measured for P, P-g-10 and P-g-20 and the results are presented on Fig. 5 (b). Initially, the raw membrane had a WCA of around 90° and this value was gradually reduced down to 70° as the number of ALD cycles increased. These results are in good agreement with literature as reported in Table 5. Indeed, Zhang *et al.* prepared PSF hybrid ultrafiltration flat membrane with TiO_2-g-HEMA and studied its antifouling characteristics. The best hydrophilicity improvement they obtained with a WCA of 72° was for 2% concentration[45].

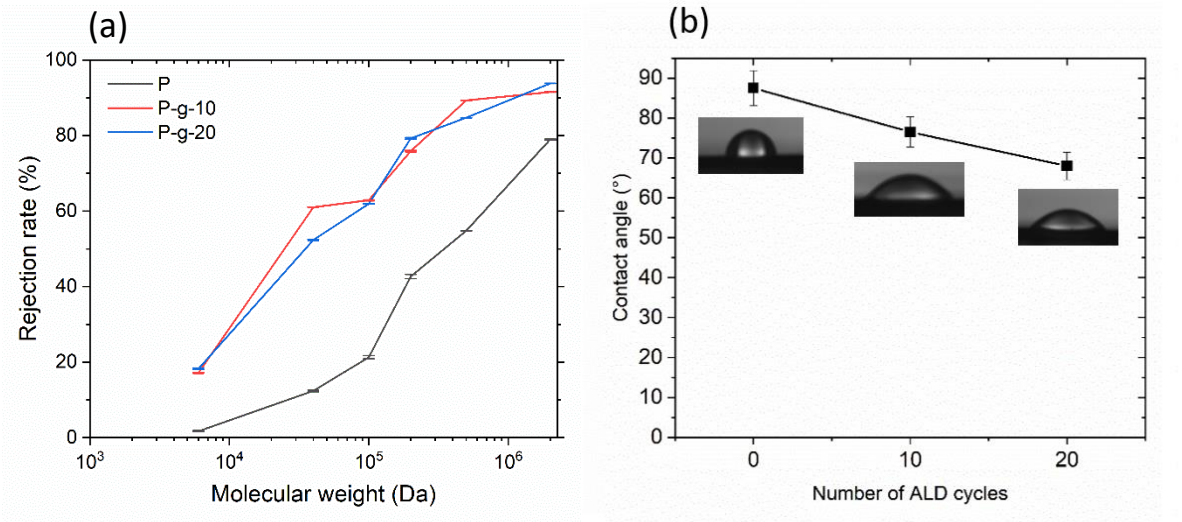

Figure 5. (a) Different sized dextran rejection rate and (b) WCA of raw and ALD modified membranes (the error referred to standard deviation of 3 samples)

The filtration performances of raw and ALD modified PSF HF membranes are depicted in Fig.6 (a). The raw membrane exhibited a pure water permeability of 135 $L{\cdot}h^{-1}m^{-2}bar^{-1}$ and a retention of BSA around 80%. However, after the ALD deposition of TiO_2, the permeability increases slightly reaching the higher value for 20 ALD cycles, then it decreases drastically for P-g-50 which displayed a water permeability of 15 $L{\cdot}h^{-1}m^{-2}bar^{-1}$. P-g-10 and P-g-20 not only showed an increased water permeability but also a higher BSA retention compared to raw PSF HF membrane. Wang et *al.* deposited TIO_2 on PVDF membranes *via* ALD process at 80°C. They observed a decrease of permeability that they attributed to the pore size diminution which is probably the result of the ALD process. Indeed, in addition to the surface, the $TiCl_4$ molecules can also penetrate into the subsurface of the membrane. Water vapors pulsed into the chamber reacted with the $TiCl_4$ entrapped in the free volumes between the polymer chains producing layers of TiO_2. When the number of ALD cycles increases, the TiO_2 keeps growing inside the membrane pores until they are completely blocked[48]. In our case, a pore size reduction was

also noticed from dextran filtration accompanied by an increase in hydrophilicity. These two combined parameters explain the membrane filtration performances. Hypothetically, during acclimation all the glycerin was slowly evaporated which prevented the pores from collapsing and maintained the internal morphology. Above 20 ALD cycles, in accordance to SEM images, the observed TiO_2 layer for P-g-50 and P-g-100 could block the pores on the membranes' surface causing the drop in water permeability.

Antifouling performances of the ALD modified membranes were investigated using BSA as a fouling agent, for that the FRR, Rt, Rr and Rir of the membranes are calculated from equations (4) to (7). All the calculated values are represented in Fig. 6 (b). FRR is at 100% for P-g-10 and P-g-20 compared to 88% for raw PSF HF membrane. This means that due to TiO_2 addition, ALD modified PSF HF membranes were recovering all the flux after BSA filtration. Indeed, all ALD modified PSF HF membranes exhibited lower R_t, furthermore interestingly the R_r decreased with the increase of the number of ALD cycles. A reducing R_r means that BSA adsorbed reversibly was removed after water backwashing, which is a good result as membranes lifetime is threatened by fouling and most of all irreversible fouling and chemical backwashing needed to clean them. R_{ir} initially at 12% for raw membrane was at 0% for both P-g-10 and P-g-20 and around 19% for P-g-50. P-g-100 was tested but the result was not detectable. On the one hand, the ALD modified PSF HF membranes demonstrated lower BSA fouling but also a 0% R_{ir} which means that all the BSA adsorbed can be removed with water backwashing. This shows that with TiO_2 the PSF HF membranes are less sensitive to BSA fouling and would have a longer lifetime. They display higher fouling resistance against protein compared to the raw PSF HF membrane. These results are very interesting since the values are even better than that reported in other studies (Table 6). Yang *et al.*[46] and Zhang *et al.*[45] inserted for instance TiO_2 nanoparticles into flat PSF membranes and obtained respectively 97 and 95% BSA rejection. Jia *et al.*[49] deposited Al_2O_3 on PP HF membranes and obtained a maximum of 75% BSA rejection.

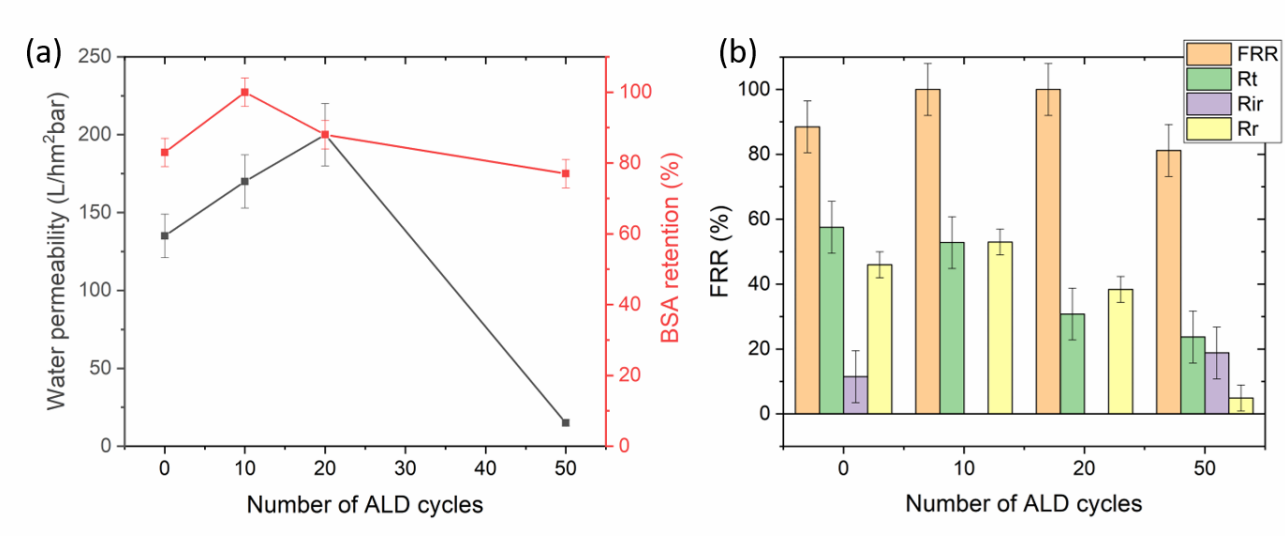

Figure 6. (a) Water permeability and BSA retention and (b) Fouling resistance parameters for raw and ALD modified membranes (the error referred to standard deviation of 3 samples)

To go further, BSA hydrodynamic radius is 10 nm and for P-g-10 40 % of corresponding Dextran molecule (Mw = 4.10^4 Da) passed through against 0 % of BSA molecule. This proved that BSA is not only rejected because of its size but thanks to the higher hydrophilicity of the membrane due to TiO_2 deposit.

Table 6. Comparison of this study with results reported in literature

reference	support	oxide	HF or flat membrane	method	Water permeability ($L.m^{-2}h^{-1}bar^{-1}$)	foulant rejection (%)	Mean pores diameter (nm)	WCA (°)
This study	PSF	TiO_2	HF	ALD 0 cycle	135	83	25	88
				ALD 10 cycles	170	100	Reduction	76
				ALD 20 cycles	200	88	Reduction	68
Hamid *et al.*[34]	PSF	TiO_2	HF	Insertion	78.33 ± 0.52	90 (HA)	47.58 ± 0.14	45
Yang *et al.*[46]	PSF	TiO_2	Flat membrane	Insertion 1wt%	400	97 (BSA)	6.9	52.6
Zhang *et al.*[45]	PSF	TiO_2	Flat membrane	Insertion 1wt%	90	95 (BSA)	18	78
Kusworo *et al.*[44]	PSF	TiO_2	Flat membrane	Insertion 1wt%	0.5	90 (NH_3)	9.05± 0.63	44.17
Cheraghi Bidsorkhi *et al.*[47]	PSF	TiO_2	Flat membrane	Insertion 1wt%	500	98 (BSA)	/	59.9
Galiano *et al.*[56]	PVDF	/	HF	Insertion 0.5wt%	280	/	130 ± 30	78 ± 2
Wang *et al.*[48]	PVDF	TiO_2	Flat membrane	ALD 30 cycles	70	85 (BSA)	40.8	65
				ALD 100 cycles	110	90 (BSA)	25.7	45
Jia *et al.*[49]	PP	Al_2O_3	HF	ALD 50 cycles	284.9	28 (BSA)	not quantified	
				ALD 200 cycles	180	75 (BSA)		

4. Conclusion

Atomic layer deposition of TiO_2 on PSF HF membranes was studied. The protective effect of glycerin to prevent pore collapsing during ALD process when the polymeric membrane is exposed under vacuum at 100°C was clearly demonstrated. By this way, TiO_2 deposit onto the surface and the porous substructure can be achieved to give better performances in terms of permeability and anti-fouling

properties with BSA. Moreover, the acclimation duration in the ALD chamber must not be too long because of the drastic reduction of glycerin boiling temperature under 10^{-2} mbar vacuum (98°C against 290°C under atmospheric pressure). The duration of the ALD process cannot be much more longer than the glycerin evaporation. Based on these conditions, different number of ALD cycles were tested from 10 to 100 corresponding to thicknesses between 1 and 10 nm. The presence of TiO_2 was proved by EDX analysis. On SEM images, TiO_2 layer was observed only upon 50 ALD cycles. Thanks to XPS analyses, the reaction between TiO_2 and the oxygen groups of PSF membranes was confirmed. Dextran molecules filtration showed a clear pore size and pore size distribution reduction for ALD modified PSF HF membranes compared to raw PSF HF membranes. Hydrophilicity improvement was confirmed by WCA reduction from 90° for raw PSF HF membrane to 70° for 20 ALD cycles modified PSF HF membranes. These two parameters explain the enhanced water filtration and fouling properties results of ALD modified PSF HF membranes. Indeed, the ones with 10 and 20 ALD cycles showed the best results, with water permeability up to 26 % higher compared to raw HF membrane and an optimum 100% FRR and a 0% $R_{ir.}$ All ALD modified PSF HF membranes' mechanical properties were not altered by ALD process. The obtained results are a first step for a more in-depth study on TiO_2 coating by ALD on PSF HF membranes. It would be interesting to open the test in real membrane measurement and for filtration of other contaminants. Finally, to the best of our knowledge, this work is a first report on TiO_2 ALD on PSF HF membranes and may pave the way for further studies.

Acknowledgment.

This project is part of INNOMEM and receives funding from the European Union's Horizon 2020 Research and Innovation Program under Grant Agreement N° 862330. Authors would like to thanks the companies Polymem for providing the PSF HF membranes and Porometer for the determination of HF membranes mean pore diameter. The authors acknowledge D. Cot and B. Rebiere for SEM and EDX observations and V. Bonniol for her technical support for Dextran analysis. Authors would like to thank Aurélien Renard from the SMI LCPME facility (Université de Lorraine-CNRS–http://www.lcpme.cnr-nancy.fr) for XPS analysis.

References

1. Kumar, M. D. & Tortajada, C. *SPRINGER BRIEFS IN WATER SCIENCE AND TECHNOLOGY Assessing Wastewater Management in India*.
2. Science, E. Water pollution Its causes and effects. (2021) doi:10.1088/1755-1315/790/1/012026.
3. Chowdhary, P. *Microorganisms for sustainable environnement and health*.
4. Review, A. Membrane Technologies in Wastewater Treatment : (2020).
5. Monsalve-bravo, G. M. & Bhatia, S. K. Comparison of hollow fiber and flat mixed-matrix membranes : Theory and simulation. *Chem. Eng. Sci.* **187**, 174–188 (2018).
6. Practice, W. & Africa, S. Membrane desalination technologies in water treatment : A review Usman Mohammed Aliyu , Sudesh Rathilal and Yusuf Makar fi Isa *. **13**, 738–752 (2018).
7. Lee, M., Wu, Z. & Li, K. *Advances in ceramic membranes for water treatment*. *Advances in*

Membrane Technologies for Water Treatment: Materials, Processes and Applications (2015). doi:10.1016/B978-1-78242-121-4.00002-2.

8. He, Z., Lyu, Z., Gu, Q., Zhang, L. & Wang, J. Ceramic-based membranes for water and wastewater treatment. *Colloids Surfaces A Physicochem. Eng. Asp.* **578**, (2019).

9. Kazemimoghadam, M. New nanopore zeolite membranes for water treatment. *Desalination* **251**, 176–180 (2010).

10. Garofalo, A. *et al.* Supported MFI zeolite membranes by cross flow filtration for water treatment. *Sep. Purif. Technol.* **137**, 28–35 (2014).

11. Subramani, A. *et al.* Recovery optimization of membrane processes for treatment of produced water with high silica content. *Desalin. Water Treat.* **36**, 297–309 (2011).

12. Chua, Y. T., Lin, C. X. C., Kleitz, F. & Smart, S. Synthesis of mesoporous carbon-silica nanocomposite water-treatment membranes using a triconstituent co-assembly method. *J. Mater. Chem. A* **3**, 10480–10491 (2015).

13. Wang, S., Wang, Z. yang, Xia, J. zhong & Wang, X. mao. Polyethylene-supported nanofiltration membrane with in situ formed surface patterns of millimeter size in resisting fouling. *J. Memb. Sci.* **620**, 118830 (2021).

14. Hosseini, S. S., Fakharian Torbati, S., Alaei Shahmirzadi, M. A. & Tavangar, T. Fabrication, characterization, and performance evaluation of polyethersulfone/TiO2 nanocomposite ultrafiltration membranes for produced water treatment. *Polym. Adv. Technol.* **29**, 2619–2631 (2018).

15. Nawi, N. I. M. *et al.* Development of hydrophilic PVDF membrane using vapour induced phase separation method for produced water treatment. *Membranes (Basel).* **10**, 1–17 (2020).

16. Rodrigues, R., Mierzwa, J. C. & Vecitis, C. D. Mixed matrix polysulfone/clay nanoparticles ultrafiltration membranes for water treatment. *J. Water Process Eng.* **31**, 100788 (2019).

17. Alresheedi, M. T., Barbeau, B. & Basu, O. D. Separation and Puri fi cation Technology Comparisons of NOM fouling and cleaning of ceramic and polymeric membranes during water treatment. *Sep. Purif. Technol.* **209**, 452–460 (2019).

18. Goh, P. S., Matsuura, T., Ismail, A. F. & Hilal, N. Recent trends in membranes and membrane processes for desalination. *DES* (2015) doi:10.1016/j.desal.2015.12.016.

19. Yong, L., Wahab, A., Peng, C. & Hilal, N. Polymeric membranes incorporated with metal / metal oxide nanoparticles : A comprehensive review. *DES* **308**, 15–33 (2013).

20. Cai, T., Li, X., Wan, C. & Chung, T. S. Zwitterionic polymers grafted poly(ether sulfone) hollow fiber membranes and their antifouling behaviors for osmotic power generation. *J. Memb. Sci.* **497**, 142–152 (2016).

21. Wan, P., Yuan, M., Yu, X., Zhang, Z. & Deng, B. Arsenate removal by reactive mixed matrix PVDF hollow fiber membranes with UIO-66 metal organic frameworks. *Chem. Eng. J.* **382**, 122921 (2020).

22. Fotovvati, B., Namdari, N. & Dehghanghadikolaei, A. On coating techniques for surface protection: A review. *J. Manuf. Mater. Process.* **3**, (2019).

23. Dong, H., Xiao, K. J., Li, X. L., Ren, Y. & Guo, S. Y. Preparation of PVDF/Al2O3 hybrid membrane via the sol-gel process and characterization of the hybrid membrane. *Desalin. Water Treat.* **51**, 3685–3690 (2013).

24. Kowalik-Klimczak, A., Stanisławek, E., Kacprzyńska-Gołacka, J., Kaźmierczak, B. & Wieciński, P. The polyamide membranes modified by copper oxide using PVD techniques. *J. Mach. Constr. Maintenance. Probl. Eksploat.* **3**, 49–55 (2018).

25. Nomura, M. *Preparation of Silica Membranes by CVD Method*. *Current Trends and Future Developments on (Bio-) Membranes: Silica Membranes: Preparation, Modelling, Application, and Commercialization* (Elsevier B.V., 2017). doi:10.1016/B978-0-444-63866-3.00002-9.

26. Pakkala, A. & Putkonen, M. *Atomic Layer Deposition*. *Handbook of Deposition Technologies for Films and Coatings* (Elsevier Ltd., 2010). doi:10.1016/B978-0-8155-2031-3.00008-9.

27. Nikkola, J. *et al.* Surface modi fi cation of thin fi lm composite polyamide membrane using atomic layer deposition method. *J. Memb. Sci.* **450**, 174–180 (2014).

28. Gao, Y. *et al.* Cooperating effects of conformal iron oxide (FeOx) ALD coating and post-annealing on Li-Rich layered cathode materials. *Electrochim. Acta* **318**, 513–524 (2019).

29. Neudeck, S. *et al.* Effect of Low-Temperature Al 2 O 3 ALD Coating on Ni-Rich Layered Oxide Composite Cathode on the Long-Term Cycling Performance of Lithium-Ion Batteries. 1–11 (2019) doi:10.1038/s41598-019-41767-0.

30. Barhate, V., Agrawal, K., Patil, V., Patil, S. & Mahajan, A. Spectroscopic study of La2O3 thin films deposited by indigenously developed plasma-enhanced atomic layer deposition system. *Int. J. Mod. Phys. B* **32**, 1–5 (2018).

31. Mione, M. A., Vandalon, V., Mameli, A., Kessels, W. M. M. & Roozeboom, F. Atmospheric-Pressure Plasma-Enhanced Spatial ALD of SiO2Studied by Gas-Phase Infrared and Optical Emission Spectroscopy. *J. Phys. Chem. C* **125**, 24945–24957 (2021).

32. Kim, H. Y. *et al.* Phase-controlled SnO2 and SnO growth by atomic layer deposition using Bis(N-ethoxy-2,2-dimethyl propanamido)tin precursor. *Ceram. Int.* **45**, 5124–5132 (2019).

33. Feng, J., Xiong, S., Ren, L. & Wang, Y. Article Atomic layer deposition of TiO 2 on carbon-nanotubes membrane for capacitive deionization removal of chromium. *Chinese J. Chem. Eng.* (2021) doi:10.1016/j.cjche.2021.05.014.

34. Hamid, N. A. A. *et al.* Morphological and separation performance study of polysulfone/titanium dioxide (PSF/TiO2) ultrafiltration membranes for humic acid removal. *Desalination* **273**, 85–92 (2011).

35. Nechifor, G. *et al.* Non-resorbable nanocomposite membranes for guided bone regeneration based on polysulfone-quartz fiber grafted with nano-TiO2. *Nanomaterials* **9**, 1–22 (2019).

36. Lee, J. & Kim, I. S. Environmental Science membrane surface engineering methods for water treatment : a short review. 1765–1785 (2020) doi:10.1039/c9ew01134j.

37. Weber, M., Julbe, A., Ayral, A., Miele, P. & Bechelany, M. Atomic Layer Deposition for Membranes : Basics , Challenges , and Opportunities. (2018) doi:10.1021/acs.chemmater.8b02687.

38. Yang, X., Martinson, A. B. F., Elam, J. W., Shao, L. & Darling, S. B. Water treatment based on atomically engineered materials: Atomic layer deposition and beyond. *Matter* **4**, 3515–3548 (2021).

39. Wu, S. L., Liu, F., Yang, H. C. & Darling, S. B. Recent progress in molecular engineering to tailor organic-inorganic interfaces in composite membranes. *Mol. Syst. Des. Eng.* **5**, 433–444 (2020).

40. Yang, H. C., Waldman, R. Z., Chen, Z. & Darling, S. B. Atomic layer deposition for membrane

interface engineering. *Nanoscale* **10**, 20505–20513 (2018).

41. Feng, J. *et al.* Atomic layer deposition of metal oxides on carbon nanotube fabrics for robust, hydrophilic ultrafiltration membranes. *J. Memb. Sci.* **550**, 246–253 (2018).

42. Wang, H., Wei, M., Zhong, Z. & Wang, Y. Atomic-layer-deposition-enabled thin-film composite membranes of polyimide supported on nanoporous anodized alumina. *J. Memb. Sci.* **535**, 56–62 (2017).

43. Parsons, G. N. *et al.* Mechanisms and reactions during atomic layer deposition on polymers. *Coord. Chem. Rev.* **257**, 3323–3331 (2013).

44. Kusworo, T. D., Ariyanti, N. & Utomo, D. P. Effect of nano-TiO2 loading in polysulfone membranes on the removal of pollutant following natural-rubber wastewater treatment. *J. Water Process Eng.* **35**, 101190 (2020).

45. Zhang, G. *et al.* Novel polysulfone hybrid ultrafiltration membrane prepared with TiO2-g-HEMA and its antifouling characteristics. *J. Memb. Sci.* **436**, 163–173 (2013).

46. Yang, Y., Wang, P. & Zheng, Q. Preparation and properties of polysulfone/TiO2 composite ultrafiltration membranes. *J. Polym. Sci. Part B Polym. Phys.* **44**, 879–887 (2006).

47. Bidsorkhi, H. C. *et al.* Preparation and characterization of a novel highly hydrophilic and antifouling polysulfone/nanoporous TiO2 nanocomposite membrane. *Nanotechnology* **27**, 1–11 (2016).

48. Wang, Q., Wang, X., Wang, Z., Huang, J. & Wang, Y. PVDF membranes with simultaneously enhanced permeability and selectivity by breaking the tradeoff effect via atomic layer deposition of TiO 2. *J. Memb. Sci.* **442**, 57–64 (2013).

49. Jia, X., Low, Z., Chen, H., Xiong, S. & Wang, Y. Atomic layer deposition of Al2O3 on porous polypropylene hollow fibers for enhanced membrane performances. *Chinese Journal of Chemical Engineering* vol. 26 695–700 at https://doi.org/10.1016/j.cjche.2017.10.008 (2018).

50. Sayegh, S. *et al.* N-doped TiO2 nanotubes synthesized by atomic layer deposition for acetaminophen degradation. *Colloids Surfaces A Physicochem. Eng. Asp.* **655**, 130213 (2022).

51. Wickramasinghe, S. R., Bower, S. E., Chen, Z., Mukherjee, A. & Husson, S. M. Relating the pore size distribution of ultrafiltration membranes to dextran rejection. *J. Memb. Sci.* **340**, 1–8 (2009).

52. Alkhouzaam, A. & Qiblawey, H. Novel polysulfone ultrafiltration membranes incorporating polydopamine functionalized graphene oxide with enhanced flux and fouling resistance. *J. Memb. Sci.* **620**, 118900 (2021).

53. Lide, D. R. & Kehiaian, H. V. *CRC HANDBOOK of THERMOPHYSICAL and THERMOCHEMICAL DATA*. *CRC HANDBOOK of THERMOPHYSICAL and THERMOCHEMICAL DATA* (CRC Press, 2020). doi:10.1201/9781003067719.

54. Cabasso, I., Klein, E., Smith, J. K. & South, G. Polysulfone Hollow Fibers . I . Spinning and Properties. **20**, 2377–2394 (1976).

55. Waldman, R. Z. *et al.* Sequential Infiltration Synthesis of Al2O3 in Polyethersulfone Membranes. *Jom* **71**, 212–223 (2019).

56. Galiano, F. *et al.* Novel photocatalytic PVDF/Nano-TiO2 hollow fibers for Environmental remediation. *Polymers (Basel).* **10**, 1–20 (2018).

57. Díez-Pascual, A. M. & Díez-Vicente, A. L. Effect of TiO2 nanoparticles on the performance of

646 polyphenylsulfone biomaterial for orthopaedic implants. *J. Mater. Chem. B* **2**, 7502–7514
647 (2014).

648